# Improving the real-time ionospheric determination from GPS sites at very long distances over the equator

M. Hernández-Pajares, J. M. Juan, and J. Sanz

Group of Astronomy and Geomatics, Department of Applied Mathematics IV and Applied Physics, Universitat Politècnica de Catalunya, Barcelona, Spain

O. L. Colombo

Goddard Earth Sciences and Technology Center, NASA Goddard Space Flight Center, Greenbelt, Maryland, USA

Received 4 December 2001; revised 13 March 2002; accepted 15 March 2002; published 15 October 2002.

[1] As the authors have shown in previous work, the tomographic approach reduces significantly the mismodeling in the electron content determination using as data the ionosphere-crossing radio signals of global navigation satellite systems (GNSS) such as the Global Positioning System (GPS). We present in this paper the results of a comprehensive study on the performance of an improved tomographic model of the ionosphere. This model is obtained from the GPS L1 and L2 carrier-phase data, and it is used to estimate undifferenced and double-differenced ionospheric corrections in real time and at very long distances between receivers (500–3000 km). The key point of the strategy is the combination of real-time geodetic and ionospheric techniques to achieve a significant improvement in the reliability of carrier-phase ambiguity resolution. This new approach includes also the use of smoothed pseudo-ranges to help in ambiguity resolution. It has been tested under difficult ionospheric conditions, during four consecutive weeks in March–April 2001, at Solar Maximum, and at latitudes ranging from −40 to +40 degrees, so as to include the equatorial region. Dual-frequency satellite altimetry from TOPEX-Poseidon has been used to verify the accuracy of the ionospheric model over the oceans in that region. *INDEX TERMS:* 2494 Ionosphere: Instruments and techniques; 2415 Ionosphere: Equatorial ionosphere; 2447 Ionosphere: Modeling and forecasting; 6934 Radio Science: Ionospheric propagation (2487); 1244 Geodesy and Gravity: Standards and absolute measurements; *KEYWORDS:* modeling and forecasting, instruments and techniques, equatorial ionosphere, ionospheric propagation, space geodetic surveys

**Citation:** Hernández-Pajares M., J. M. Juan, J. Sanz, and O. L. Colombo, Improving the real-time ionospheric determination from GPS sites at very long distances over the equator, *J. Geophys. Res.*, *107*(A10), 1296, doi:10.1029/2001JA009203, 2002.

## 1. Introduction

[2] As demonstrated in recent years, it is possible to provide ionospheric corrections from global navigation satellite systems (GNSS) such as GPS, using global ionospheric maps (GIM's) computed from GPS data [see, e.g., *Wilson et al.*, 1995]. In the case of real-time applications such as wide-area navigation augmentation systems (WAAS, EGNOS, MSAS [see, e.g., *El-Arini et al.*, 1995]) the ionospheric corrections have to be calculated from receiver data collected at stations typically separated by several hundreds of kilometers using only data gathered until the present epoch. This real-time limitation usually produces less precise results than when postprocessing all the data collected during a long observing session. One way to overcome this natural limitation is to run, simultaneously with the ionosphere-modeling procedure, a geodetic program to solve for a number of nuisance parameters (errors in orbits, site coordinates, tropospheric refraction model, etc.) so as to estimate very precisely the biases in the carrier-phase ionosphere-free combination, Lc. By using these procedures together, both the ionospheric corrections and also the geodetic outputs can improve significantly. Some examples of this can be found in *Hernández-Pajares et al.* [2000b] for ionospheric corrections, in *Colombo et al.* [1999] for navigation and in *Hernández-Pajares et al.* [2001] for real-time tropospheric determination.

[3] The purpose of this paper is to show the benefit of combining precise real-time ionospheric modeling, with a tomographic approach, a precise geodetic analysis, in a more difficult scenario than encountered in our past work. We deal here with GPS sites separated by thousands of kilometers across the equatorial region, where the ionospheric electron density presents the largest values and strongest spatial and temporal gradients, under solar maximum conditions. At such very long distances, this strategy can help improve the accuracy in the real-time global ionospheric maps that may be produced as a result of a shift of the International GPS


0148-0227/02/2001JA009203$09.00

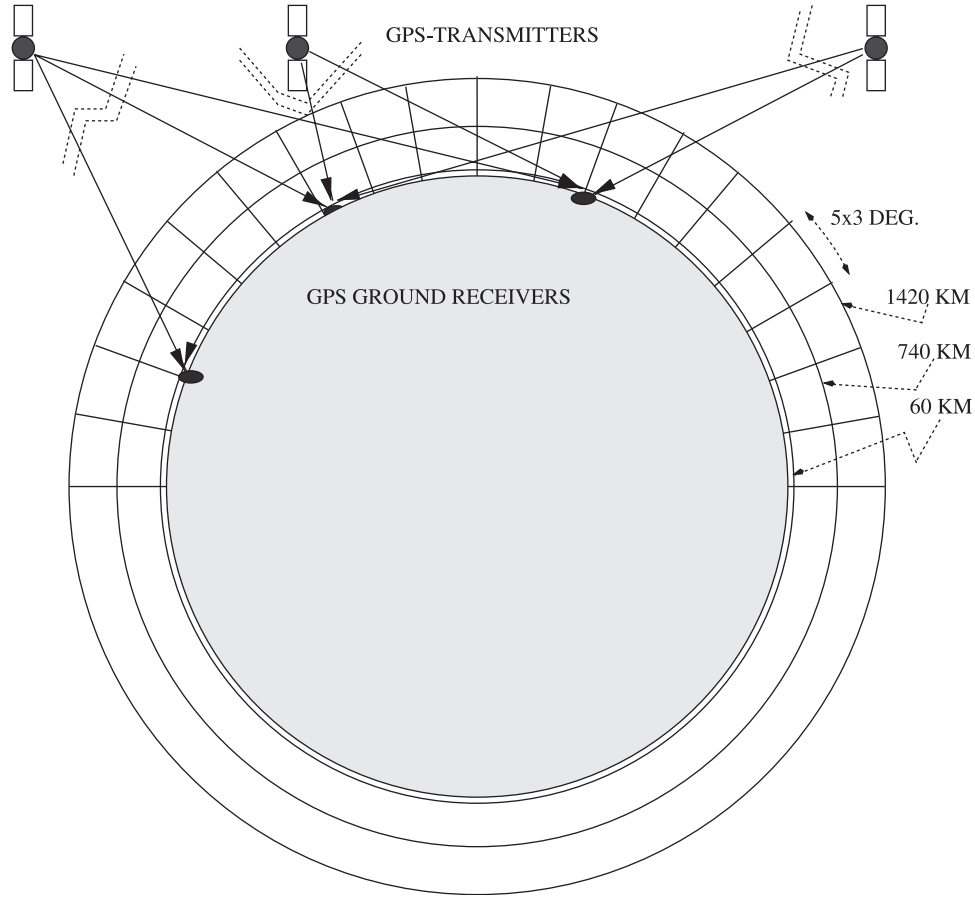


**Figure 1.** Meridian slice of the constant-density voxels into which the ionospheric electron density distribution is divided in the GNSS data-driven real-time model (equation (3)).

Service (IGS) towards real-time capabilities [*Zumberge et al.*, 1999]. These maps can help improve the accuracy for single-frequency users as well.

[4] This paper is organized as follows: In the first part, the technique is described. In the second part experiments showing the improvement in the availability of the precise ionospheric corrections are presented in detail. In one four-week long experiment in the tropics, in 2001, we have tested the improvement in the real-time ionospheric model, using data from GPS permanent stations from one thousand to three thousand kilometers apart during the seasonal maximum of the diurnal TEC, with high solar activity. The results have been verified over land using data from one station not included in the model, and at sea, using dual-frequency altimeter data from the TOPEX-Poseidon satellite.

## 2. Description of the Technique

[5] The free electron ionospheric distribution is approximated by a grid of voxels in which the electron density is assumed constant at a given time in an Earth Centered Inertial (ECI) system (see a typical layout in Figure 1). A grid with two layers, and 5 × 3 deg in local time and latitude represents a compromise between precision (about 1 TECU, needed to solve the carrier-phase ambiguities in real time [*Hernández-Pajares et al.*, 1999b] and computation load (about 6000 unknowns involved).

[6] The ionospheric determination is performed solving in real-time equation (3), by means of a Kalman Filter [*Bierman*, 1977; *Hernández-Pajares et al.*, 1998, equation (3)], such that described in equation (1):

$$x(t+\Delta t) = x(t) + K \cdot [y(t+\Delta t) - \hat{y}(t+\Delta t)] \qquad (1)$$

being $x(t)$, $x(t+\Delta t)$ the unknown (column) vectors at epochs $t$ and $t+\Delta t$; $y, \hat{y}$ the observed datum (scalar) and the predicted observation with the model, respectively; $K$ the gain vector, computed as

$$K = \left(\frac{1}{\sigma^2 + aC_{x0}\,a^t}\right) C_{x0} \cdot a^t \qquad (2)$$

being $a$ the gradient (row) vector, containing the coefficients of the model unknowns to explain observation $y(t)$; and $C_{x0}$ the covariance matrix of the a priori unknown values $x_0 \equiv x(t)$ that incorporates the possible random process variance increase; and $\sigma^2$ is the $y$ datum variance.

[7] The mean electron density $(N_e)_{i,j,k}$ of each illuminated cell $i,j,k$ (in solar longitude, latitude and height respectively), is treated as a random walk process, and with typical process noise of $10^9 - 10^{10}$ electrons/m$^3$/$\sqrt{\text{hour}}$, that is equivalent in our case (two layers with a total width of 1360 km) to a change of about $0.1 - 1$ TECU/$\sqrt{\text{hour}}$. This is an adequate value under many different ionospheric conditions, 5 to 15 times greater than the datum a priori

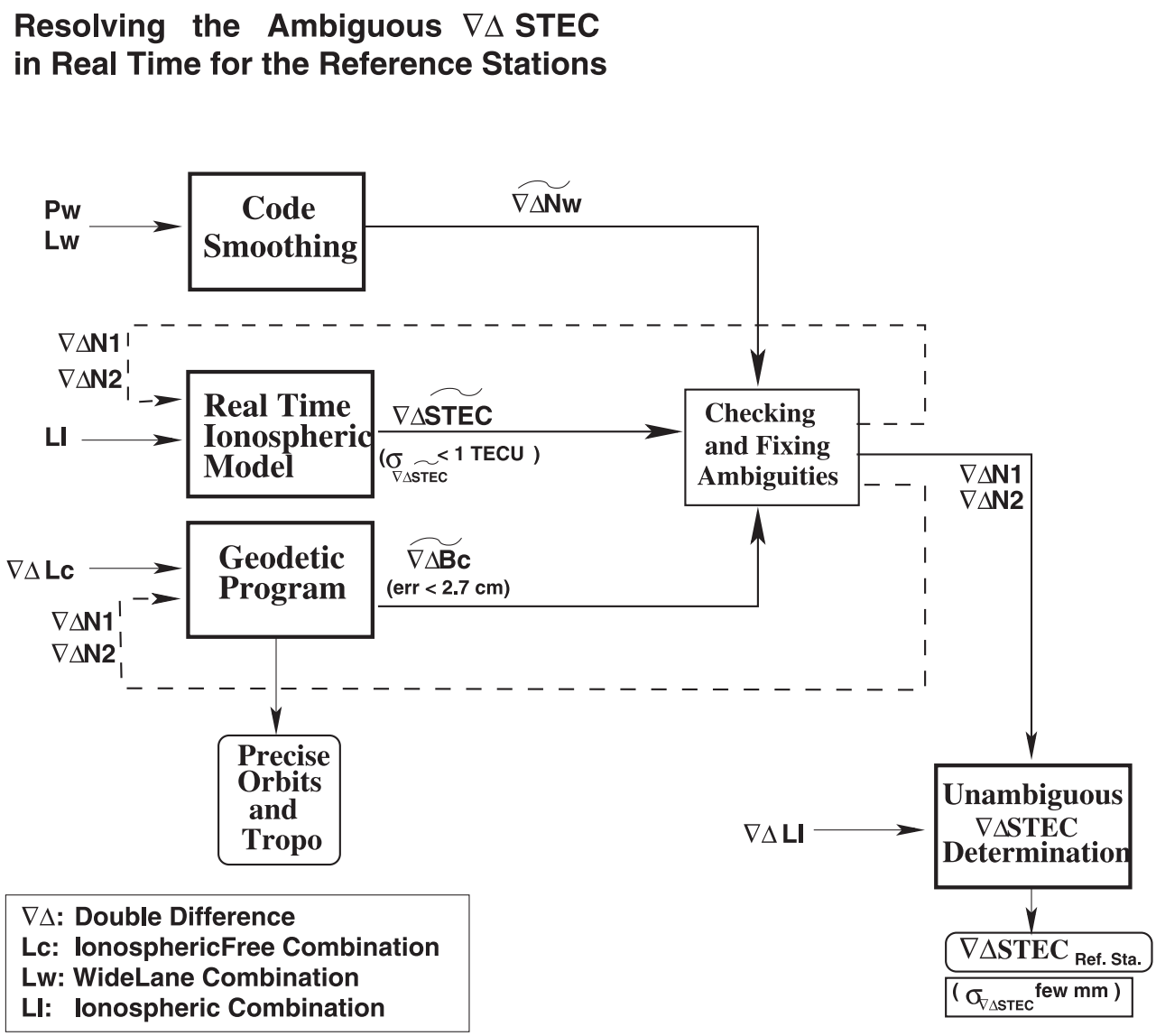


**Figure 2.** Flow diagram of the main processing steps for the reference stations.

standard deviation, being this relationship similar to those used by *Mannucci et al.* [1998]. The carrier-phase data ($L_I = L_1 - L_2$, in length units) are the main observations used. Previously, we have used no pseudo-range data, because of their much grater noise and multipath problems, compared to the carrier phase. For this work, we have used it only to a limited extent, in the form of phase-smoothed pseudo-range. The carrier-phase biases $B_I$ (constant in each continuous arch of carrier-phase data with the same satellite-receiver pair) are estimated simultaneously as random variables (restarted whenever there is a cycle slip). In the filter the biases $B_I$ decorrelate in real time from the electron density values $N_e$ as long as the satellite geometry changes and the variance of both kinds of unknown became smaller, taking into account the relationship for each ray:

$$L_I = \alpha STEC + B_I = \alpha \int_{Receiver}^{Satellite} N_e\, dl + B_I \simeq \simeq \alpha \sum_i \sum_j \sum_k (N_e)_{i,j,k} \delta l + B_I \quad (3)$$

being $\alpha \simeq 1.05$ (meters $L_I$)/($10^{17}$ electrons $\cdot$ m$^{-2}$).

[8] The filter starts assimilating data from the permanent sites several hours ahead of the intended utilization period, optimizing the unknowns management, in order to assure accurate real-time estimation with well-converged filter parameters.

[9] This approach is particularly suitable for detecting local features of the electron density distribution. The use of two layers of voxels in the model –instead of one as it is usually done– reduces significantly the mismodeling of the electron content [*Hernández-Pajares et al.*, 1999a, 1999b].

[10] In the case of Wide Area Differential GNSS (WADGNSS) networks, from these real-time slant total electron content (STEC) corrections obtained by equation (1), it is possible to form the station-satellite double differences, $\nabla\Delta STEC$, and to obtain a second ambiguity (the widelane) in the reference stations (see flow chart in Figure 2). At that point, these accurate double differenced ionospheric corrections can be broadcast to any roving receiver in the WADGNSS region to help users determine their positions more precisely, by fixing the carrier-phase

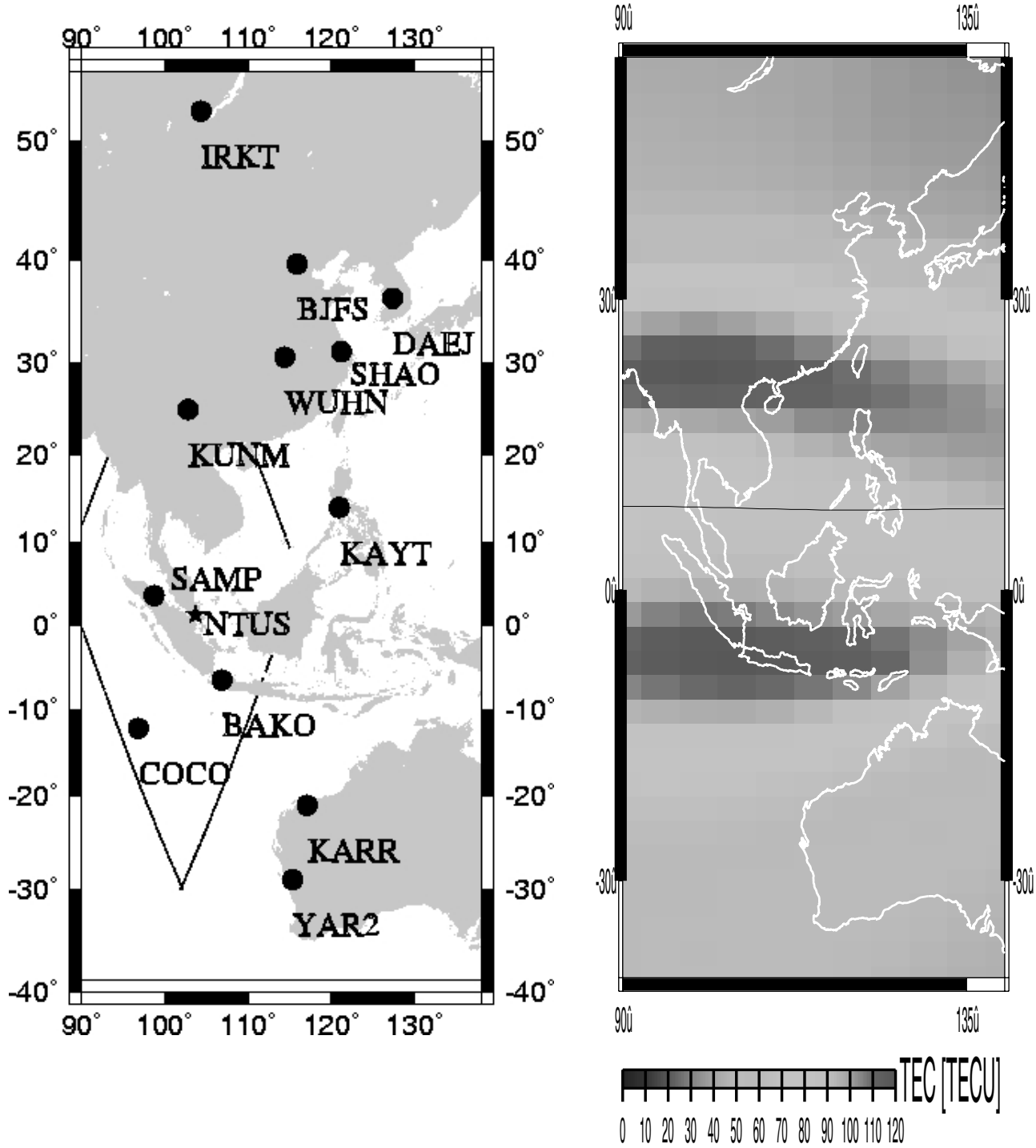


**Figure 3.** Left map: IGS stations used in the study of precise ionospheric determination, during the four consecutive weeks between March and April 2001 (the TOPEX tracks for the day 67 are also plotted). Right map: The TEC during the local afternoon (07UT, day of year [DOY] 67, March 8th, 2001). The geomagnetic equator is also shown. The units are TECU (1 TECU = 10**16 electrons/m**2 $\simeq$16.3 cm in L1). The Appleton north and south tropical anomalies are clearly present, where the TEC reaches values of more than 120 TECU, compared to 90 TECU between them, and 60 TECU or less in the north and south edges of the map (source: UPC's GIM). See color version of this figure at back of this issue.

ambiguities in their receiver data. This and other details of the technique, hereinafter called Wide Area Real Time Kinematics (WARTK), can be found, for instance, in *Hernández-Pajares et al.* [2000a, 2000b].

[11] In the case of the reference stations calculation, the long distances and the strong electron content gradients limit the performance of the technique. For this reason, we extend in this paper the algorithm to include the case of

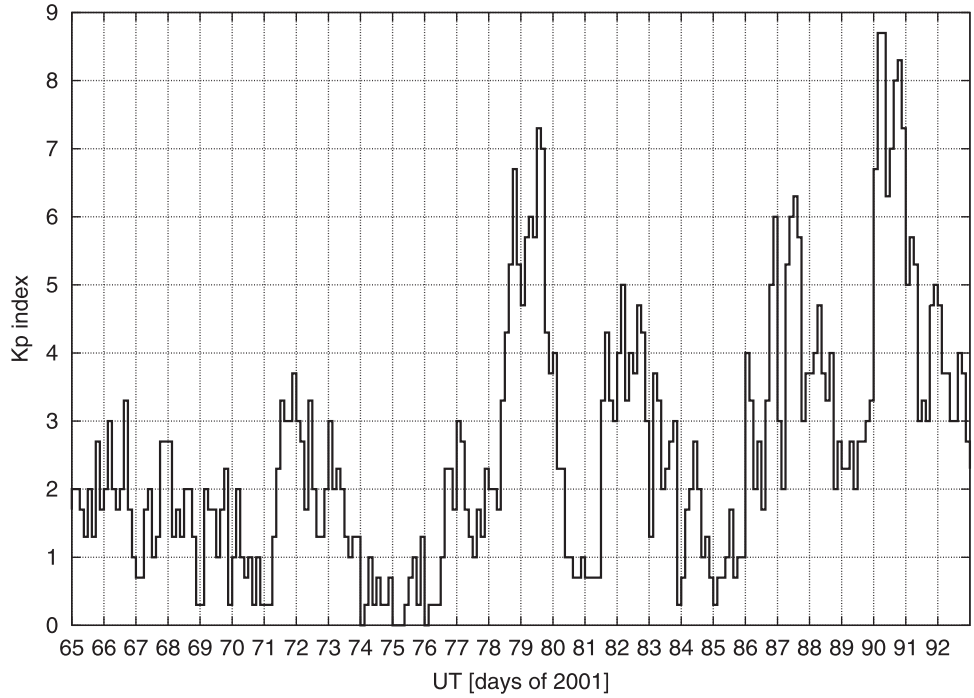


**Figure 4.** Kp index reflecting the global geomagnetic activity for the period of 4 consecutive weeks of the study described in Figure 3. During the first two weeks, approximately (DOY's 65–77), the geomagnetic activity was low to moderate (Kp < 4). However, in the last two weeks (DOY's 78–92), the geomagnetic activity attained high and geomagnetic-storm-level values in certain periods, with 6 < Kp < 9.

reference stations separated by thousands of kilometers, using also widelane-smoothed pseudo-range to improve the ionospheric model and, hence, help achieve real-time ambiguity determination.

[12] The technique can be summarized in several steps (see flow chart in Figure 2):

1. The input GPS data ($L_1$, $L_2$ carrier phases [in length units] and the corresponding pseudo-ranges $P_1$ and $P_2$, ephemeris information, coordinates of fixed sites, etc. . .) are analyzed with three programs running simultaneously in real time:

*Ionospheric program:* It processes data in the form of the geometry-free ionospheric combination of carrier phases ($L_I = L_1 - L_2$) and of transmitter-receiver rays geometry. The outputs are the estimated unknowns of the ionospheric model explained above: the mean voxel densities and the $L_I$ biases ($B_I$).

*Geodetic program:* From geometric (ionospheric-free) combination of carrier phases ($L_c = (f_1^2 L_1 - f_2^2 L_2)/(f_1^2 - f_2^2)$ being $f_1$ and $f_2$ the two corresponding frequencies) the program provides several main outputs: Improved GPS ephemeris, Zenith Tropospheric Delays (ZTD) and the $L_c$ biases of each observation ($B_c$).

*Code smoothing program:* It computes the widelane carrier-phase ambiguities ($L_w = (f_1 L_1 - f_2 L_2)/(f_1 - f_2)$) using the appropriate pseudo-ranges ($P_w = (f_1 P_1 + f_2 P_2)/(f_1 + f_2)$). These pseudo-range values are corrected by a multipath model continuously computed for each fixed site with GPS data from previous days.

2. In this way, and at a given epoch, we have three different ambiguities (ionospheric, ionospheric-free and widelane) estimated independently for each double differenced observation (between pairs of satellites and receivers). These three ambiguities are not independent from each other, as they are related to the $L_1$ and $L_2$ ambiguities ($N_1$ and $N_2$):

$$\begin{cases} \nabla\Delta B_I = \lambda_1 \nabla\Delta N_1 - \lambda_2 \nabla\Delta N_2 \\ \nabla\Delta B_c = \beta \cdot (\lambda_2 \nabla\Delta N_1 - \lambda_1 \nabla\Delta N_2) \\ \nabla\Delta B_w = \lambda_w \cdot (\nabla\Delta N_1 - \nabla\Delta N_2) = \lambda_w \cdot \nabla\Delta N_w \end{cases} \quad (4)$$

being $N_w$ the integer widelane ambiguity, $\beta = \lambda_1\lambda_2/(\lambda_2^2 - \lambda_1^2)$ and $\lambda_X$ the $X$ combination wavelength.

3. Each one of these ambiguities follows an exact relationship with the other two, that can be derived from equation (4). This allows a check on the integrity of all three ambiguities. Moreover, at this step, and for each pair of ambiguities, an additional test and computations are made following the relationships described in *Hernández-Pajares et al.* [2000a].

4. If the set of ambiguities passes the tests just described, then the ambiguities are fixed and used as additional inputs to the Ionospheric and Geodetic programs.

## 3. Experiment and Data Description

[13] Until now the strategy discussed here has been used successfully only at mid and high latitudes, with typical distances of 100–500 km between receivers, under various ionospheric conditions [*Colombo et al.*, 1999, 2000; *Hernández-Pajares et al.*, 2000a, 2000b, 2001].

[14] The goal of this new experiment is to assess the performance of the real-time ionospheric model at greater distances, 1000–3000 km, over a wider range of latitudes

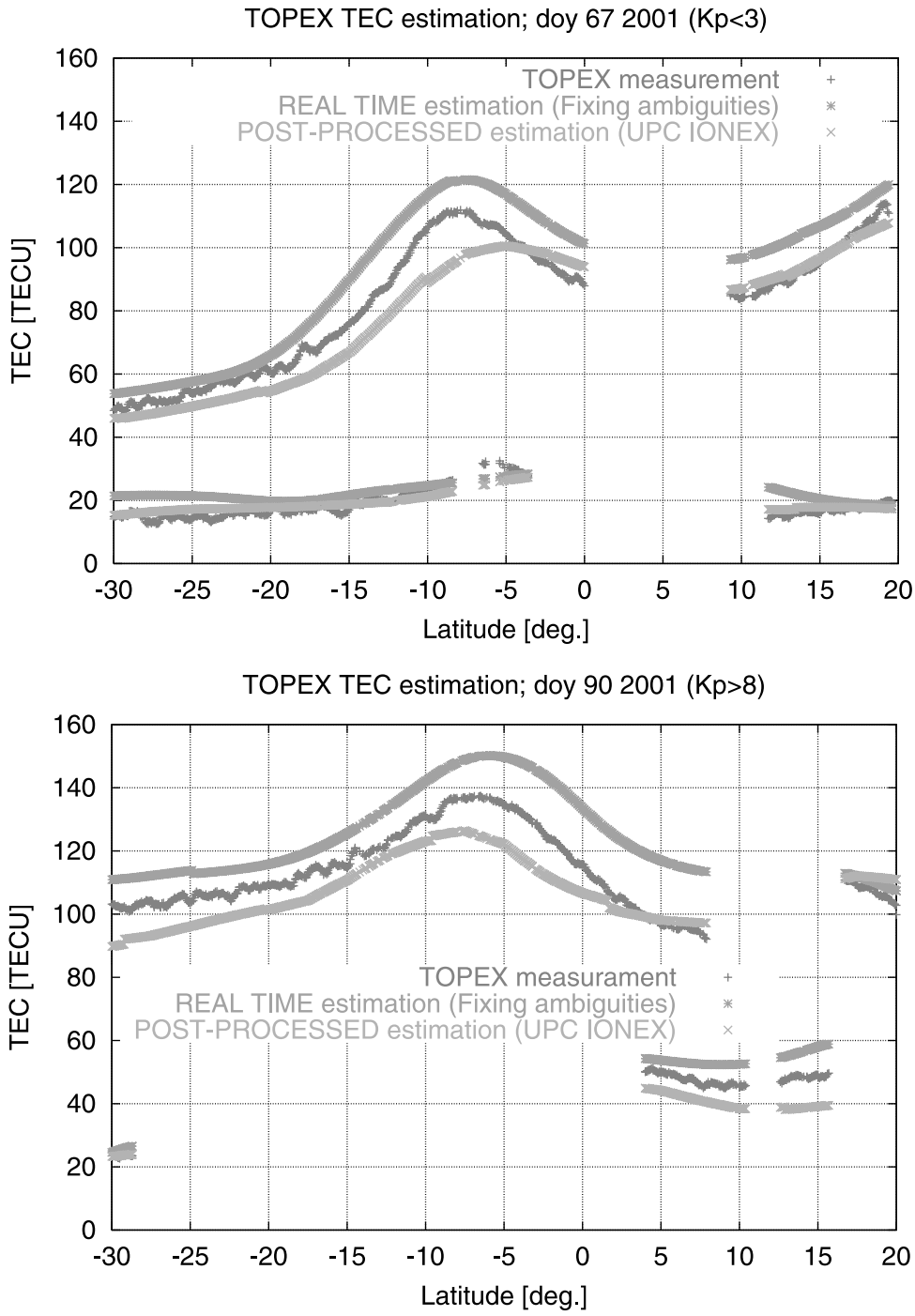


**Figure 5.** Comparison of real-time ionospheric vertical TEC determination, and postprocessed solution, both with GPS data, and TOPEX-derived TEC for four tracks in a geomagnetically quiet day (March 8th, 2001, top plot, see the four TOPEX tracks in Figure 3), and in a day geomagnetically very disturbed, with Kp $\simeq$ 8 (March 31st, 2001, lower plot). See color version of this figure at back of this issue.

and over a longer period of time, including very active ionospheric conditions.

[15] The data came from 12 permanent IGS sites in Asia and Australia, shown on the map in Figure 3. The TOPEX-Poseidon TEC observations (affected by an ionospheric error of 2–3 TECU $\simeq$0.5 cm for TOPEX altimetry [see, e.g., *Benada*, 1997, section 4]) are also used as "truth" (see typical satellite-ground tracks in the same figure). As seen in Figure 3, the satellite data cover both ionospheric equatorial anomalies, and the distances between sites are in the range of 1000–3000 km.

[16] The data period spans four whole consecutive weeks, from March 6th to April 2nd of 2001 (days of the year 65 to 92), i.e. close to the Solar Maximum, and includes the

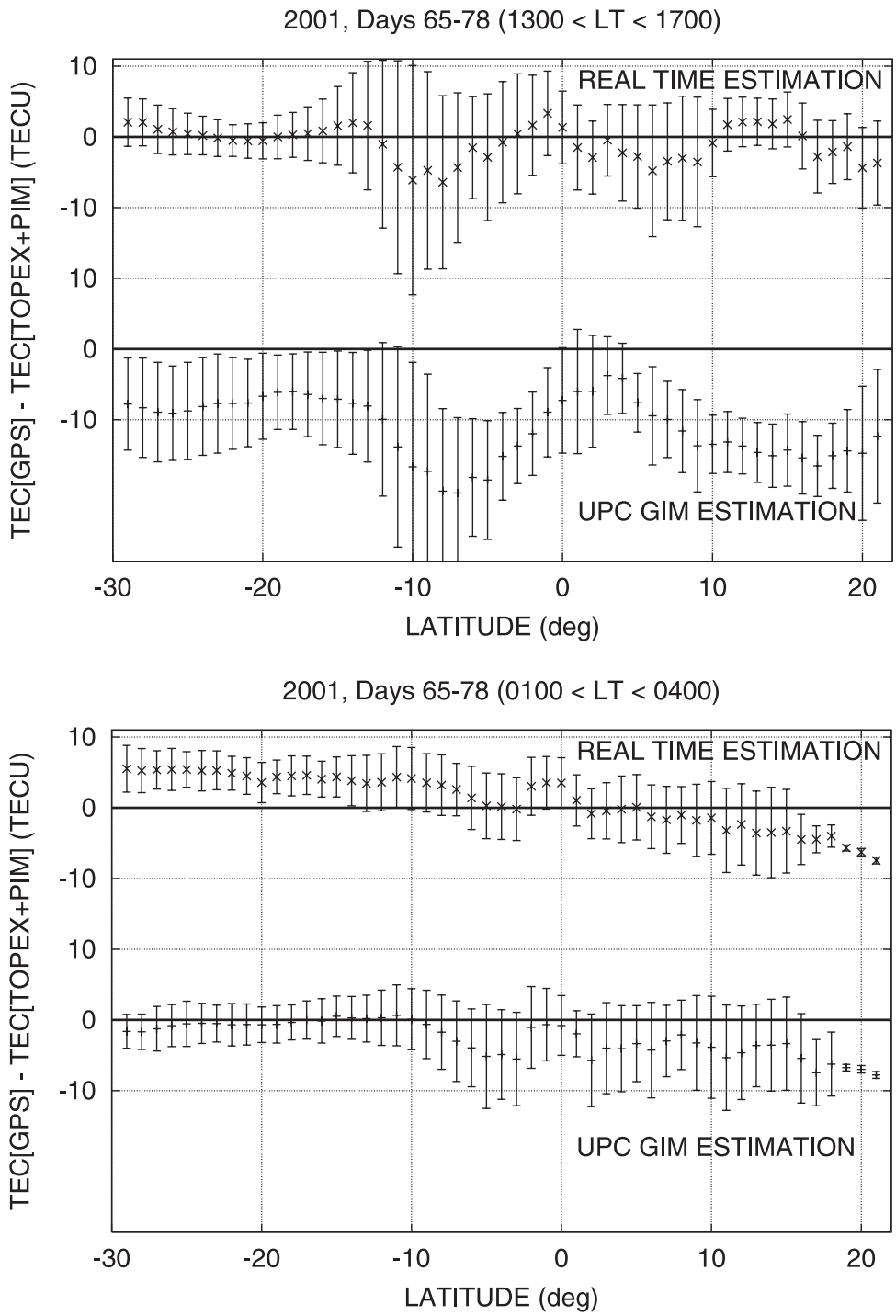


**Figure 6.** Bias and standard deviation (represented as bar errors) of the differences between GPS TEC and TOPEX TEC (corrected for plasmaspheric effects with PIM) for the first part of the studied period with low geomagnetic activity, before DOY 78, March 19th, 2001, during the local afternoon (13–17LT), and during the local night (01–04LT). Similar results are obtained with higher geomagnetic activity (starting on DOY 78).

Spring seasonal maximum of the diurnal TEC, and several disturbed periods (see Kp index in Figure 4).

## 4. Computation and Results

[17] As shown in the works mentioned earlier, ambiguity resolution requires the accuracy of the $\nabla\Delta STEC$ correction for the rover to be better than 2TECU (i.e, a one-sigma precision of 1 TECU). Furthermore, with distances of less than 1000 km between reference stations an ambiguity success rate higher than 90% can be obtained. This is better by about 10% than when using the smoothed pseudo-range alone to calculate the wide-lane ambiguity [see, e.g., *Hernández-Pajares et al.*, 1999b, Figure 16].

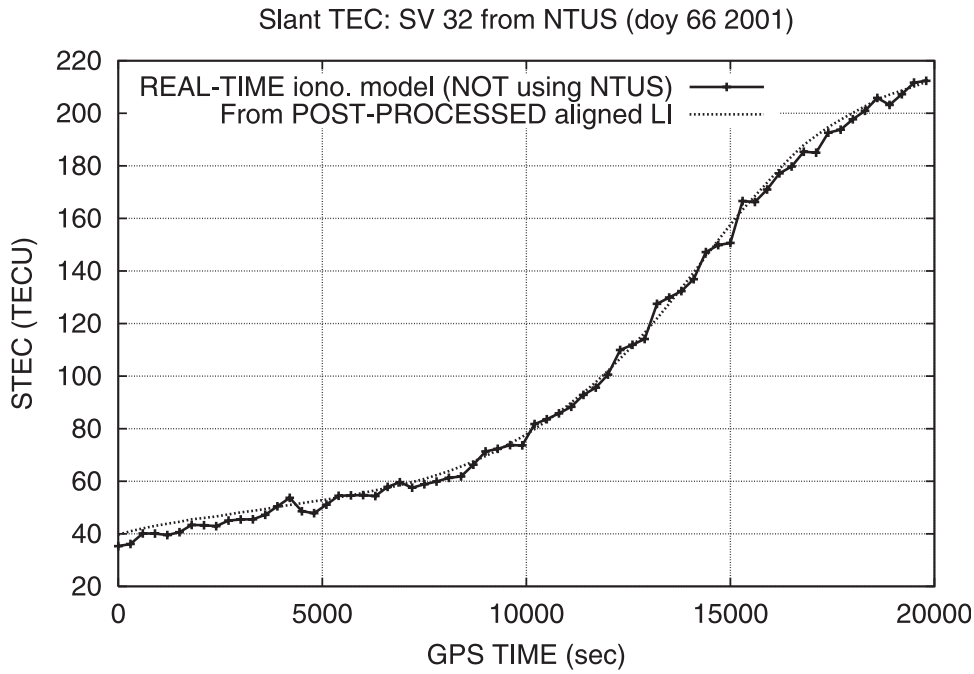


**Figure 7.** STEC predicted for NTUS, an IGS station not involved in the real-time determination over Asia and Australia, during the day March 7, 2001 (DOY 66, 2001), compared with the postprocessed solution using NTUS data from aligned ionospheric carrier phases. The maximum deviations of the predictions are lower than about 5 TECU, with a RMS of 2.8 TECU, or $\simeq$3% of the mean TEC.

However, at still greater distances (more than 1000 km) and with larger ionospheric variations, one should expect a lower percentage of success. In this case the smoothed pseudo-range can be useful to help fix the widelane ambiguities, to constrain the estimation of the real-time ionospheric model.

[18] The main problem using smoothed pseudo-range is the presence of multipath, caused by reflected signals that

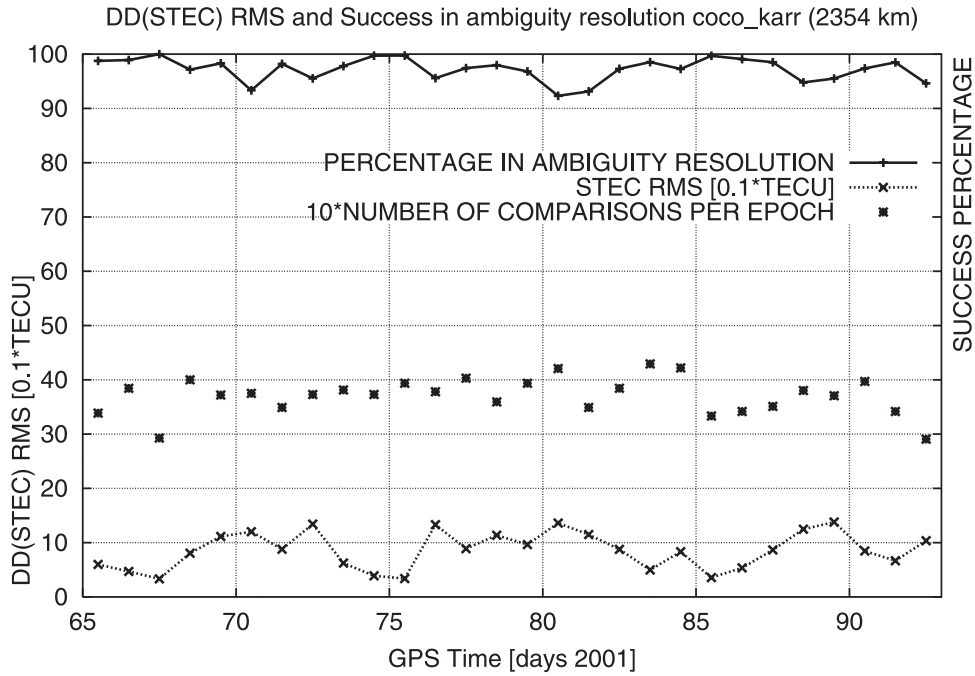


**Figure 8.** An example of the RMS of the $\nabla\Delta STEC$ real-time determination, and associated percentage of success in double-differenced widelane ambiguity resolution, for the baseline from COCO (in the southern Appleton anomaly *footprint*) to KARR in Australia (2354 km away, bottom plot) from 6 March to April 2, 2001. The mean number of observations is also plotted for each day.

**Table 1.** RMS of the $\nabla\Delta STEC$ Real-Time Determination, and Associated Percentage of Success for the Double-Differenced Widelane Ambiguity, for a Set of Representative Baselines[a]

| Station | Reference | Distance, km | Percent Success | RMS [TECU] | Number Observations |
|---|---|---|---|---|---|
| IRKT | DAEJ | 2507 | 93 | 1.2 | 8329 |
| BJFS | DAEJ | 1067 | 91 | 1.4 | 8131 |
| KUNM | DAEJ | 2640 | 95 | 1.0 | 3900 |
| WUHN | DAEJ | 1369 | 92 | 1.4 | 6358 |
| SAMP | KARR | 3341 | 95 | 1.1 | 6441 |
| COCO | KARR | 2354 | 97 | 0.9 | 9963 |
| BAKO | KARR | 1939 | 90 | 1.5 | 6121 |
| YAR2 | KARR | 909 | 97 | 0.8 | 12630 |

[a] The distance, in kilometers, and the number of observations are also indicated.

arrive later to the receiver than the direct transmission from the GPS satellite. For permanently installed receivers, it is possible to choose a good antenna location to mitigate this problem. And it is also possible to use the receiver data to estimate the actual antenna multipath pattern in order to correct much of this unwanted effect. Only for three of the more affected permanent receivers used (BJFS, KAYT and SHAO) has been computed a multipath model for correcting their pseudo-range.

[19] The precision of the real-time ionospheric corrections, based on carrier-phase data from reference stations, can be assessed in three different ways, for the vertical TEC, the STEC and the $\nabla\Delta STEC$.

[20] First, they are compared to the available precise TEC estimates obtained directly from the dual-frequency altimeter on the TOPEX-Poseidon satellite [*Benada*, 1997] over seas close to the GPS permanent receivers (Figure 3).

[21] Two examples of direct comparison of vertical TEC are shown in Figure 5, for geomagnetically quiet and very active conditions (days 67 and 90, 2001, with Kp in the ranges 0–3 and 6.5–8.5 respectively, see Figure 4). In general the real-time GPS-derived TEC follows the main trends of the TOPEX-derived TEC, but with higher values. This discrepancy is compatible with the presence of a plasmaspheric electron content of several TECU between the altimeter and the GPS satellites [*Lunt et al.*, 1999]. Remarkably, the real-time performance can be better than that of some postprocessed results, such as the GIM's distributed by UPC (see *Hernández-Pajares et al.* [1999a] for more details), or the GIM's available from other centers (in IONEX format, on-line at ftp://cddisa.gsfc.nasa.gov/pub/gps/products/ionex/YEAR/DOY). One of the reasons for this is the improvement due to fixing the ambiguities in the fixed-site carrier-phase data in real time (Figure 2), that provides very accurate values of $\nabla\Delta STEC$ to the real-time model. At present this is not yet done for the distributed UPC GIM's. Another difference is the poorer temporal resolution (2 hours) of the distributed global maps of the ionosphere, which have to be linearly interpolated in time for comparison purposes.

[22] A summary of this comparison for the first two weeks of this study, with lower geomagnetic activity, confirms these conclusions. Figure 6 shows the bias and standard deviation of the difference TEC[GPS]-TEC[TOPEX] plotted as a function of latitude, and subtracting the TOPEX topside electron content predicted by the Parameterized Ionospheric Model (PIM [*Daniell et al.*, 1995]). The two plots of Figure 6 correspond to the two daily TOPEX passes near local noon (top plot) and local night (bottom plot), with TOPEX observations relatively close to GPS stations. It can be seen the compatibility of the real-time TEC determination with TOPEX data, in particular in the diurnal passes with an accuracy better than the post-processed solutions that do not fix the carrier-phase ambiguities. Similar results are obtained for the last two weeks with higher geomagnetic activity.

[23] A second comparison can be made between the ground-site observed unambiguous STEC value (estimated in postprocessed mode) with its real-time prediction, for a receiver that has not been used in the computation of the model. This is the case of the IGS station NTUS, separated by approximately 600 km from the nearest station, SAMP (see map in Figure 3). The variation of STEC can be predicted to better than 5 TECU in a typical case, with a RMS of 2.8 TECU (3% of the mean TEC, Figure 7). This result is compatible with the vertical TEC comparison with TOPEX.

[24] Finally, in a third study of the performance of this approach, the RMS of the error in $\nabla\Delta STEC$ prediction has been calculated using as "truth" the ambiguities fixed in a postprocessed solution, to determine the corresponding real-time success rate in widelane ambiguity resolution (see flow chart in Figure 2). Figure 8 shows the results for a baseline of 2354 km (COCO-KARR), under the influence of the southern Appleton anomaly. The $\nabla\Delta STEC$ RMS is typically about 1TECU, and depends on the success rate, which is greater than the 90% during the four consecutive weeks of the period studied, with a mean rate of 97%. That period includes days of high geomagnetic activity, as shown in Figure 4. These results are quite representative, as it can be seen in Table 1, for long baselines, and for both northern and southern tropical ionosphere.

## 5. Summary and Conclusions

[25] The Wide Area Real Time Kinematic (WARTK) algorithm performs well when used to compute precise real-time ionospheric corrections in WADGPS-like networks. In several experiments previously reported in other publications, we have shown how the WARTK procedure can provide $\nabla\Delta STEC$ better than 2.7cm (1/4 TECU) for the reference and rover receivers, in middle and high latitudes, and under different ionospheric conditions [*Colombo et al.*, 1999, 2000; *Hernández-Pajares et al.*, 2000a, 2000b, 2001].

[26] In the present work, we investigate the improvement in real-time STEC determination for the reference GPS stations in one of the worst possible scenarios: Very long baselines (1000–3000 km), at low latitudes, and near-Solar Maximum conditions, during four consecutive weeks, including periods of high geomagnetic activity (March–April 2001). The vertical TEC prediction for the TOPEX-Poseidon satellite made with this method is larger than the TEC actually observed with the TOPEX-Poseidon dual frequency altimeter. This discrepancy is compatible with the existence of a significant plasmaspheric electron content between the TOPEX and the GPS satellites. This result is more compatible with TOPEX than those based on the postprocessed global-scale models (GIM's), obtained without fixing ambiguities. The standard deviation of the dis-

crepancies with the TOPEX vertical TEC is at the level of 1–3 TECU. This result is compatible with the agreement observed between measured and predicted STEC for GPS receivers not involved in the computations. Finally, in this study the RMS of the difference between the $\nabla\Delta STEC$ and the postprocessed "truth" is about 1 TECU, and the success rate in ambiguity resolution is greater than 90%. Similar results have been achieved for pairs of stations separated by more than 2000 km, and experiencing the strong gradients of the southern equatorial anomaly.

[27] **Acknowledgments.** The authors are grateful to the International GPS Service and cooperating organizations, for making publicly available the IGS data sets. The maps have been generated with the software package GMT [*Wessel and Smith*, 1995]. Some geodetic calculations were made using the GIPSY software [*Webb and Zumberge*, 1997]. This work has been partially supported by the Spanish projects TIC-2000-0104-P4-03 and TIC-2001-2356-C02-02.

[28] Arthur Richmond thanks M. Bakry El-Arini and another reviewer for their assistance in evaluating this paper.

## References

Benada, J. R., TOPEX/Poseidon Users' Handbook, Version 2.0, D-11007, http://podaac.jpl.nasa.gov/cdrom/mgdr-b/Document/HTML/usr_toc.htm, NASA JPL Phys. Oceanogr. (PODAAC) DAAC, Pasadena, Calif., 30 July 1997.

Bierman, G. J., *Factorization Methods for Discrete Sequential Estimation*, *Math. Sci. Eng. Ser.*, vol. 128, Academic, San Diego, Calif., 1977.

Colombo, O. L., M. Hernández-Pajares, J. M. Juan, J. Sanz, and J. Talaya, Resolving carrier-phase ambiguities on the fly, at more than 100 km from nearest site, with the help of ionospheric tomography, paper presented at ION GPS '99, Inst. of Navig., Nashville, Tenn., 14–17 Sept. 1999.

Colombo, O. L., M. Hernández-Pajares, J. M. Juan, and J. Sanz, Ionospheric tomography helps resolve GPS ambiguities on the fly at distances of hundreds of kilometers during high geomagnetic activity, paper presented at Position Location and Navigation Symposium 2000, Inst. of Electr. and Electron. Eng., San Diego, Calif., 12–16 March 2000.

Daniell, R. E., L. D. Brown, D. N. Anderson, M. W. Fox, P. H. Doherty, D. T. Decker, J. J. Soijka, and R. W. Schunk, Parameterized ionospheric model: A global ionospheric parameterization based on first principles models, *Radio Sci.*, *30*, 1499–1510, 1995.

El-Arini, M. B., R. S. Conker, T. W. Alberston, J. K. Reagan, J. A. Klobuchar, and P. H. Doherty, Comparison of real-time ionospheric algorithms for a GPS Wide-Area Augmentation System (WAAS), *J. Inst. Navig.*, *41*(4), 393–414, 1995.

Hernández-Pajares, M., J. M. Juan, J. Sanz, and J. G. Solé, Global observation of the ionospheric electronic response to solar events using ground and LEO GPS data, *J. Geophys. Res.*, *103*, 20,789–20,796, 1998.

Hernández-Pajares, M., J. M. Juan, and J. Sanz, New approaches in global ionospheric determination using ground GPS data, *J. Atmos. Sol. Terr. Phys.*, *61*, 1237–1247, 1999a.

Hernández-Pajares, M., J. M. Juan, J. Sanz, and O. L. Colombo, Precise ionospheric determination and its application to real-time GPS ambiguity resolution, paper presented at ION GPS '99, Inst. of Navig., Nashville, Tenn., 14–17 Sept. 1999b.

Hernández-Pajares, M., J. M. Juan, J. Sanz, and O. L. Colombo, Application of ionospheric tomography to real-time GPS carrier-phase ambiguities resolution, at scales of 400–1000 km and with high geomagnetic activity, *Geophys. Res. Lett.*, *27*, 2009–2012, 2000a.

Hernández-Pajares, M., J. M. Juan, J. Sanz, O. Colombo, and H. van der Marel, Real-time integrated water vapor determination using OTF carrier-phase ambiguity resolution in WADGPS networks, paper presented at ION GPS '2000, Inst. of Navig., Salt Lake City, Utah, 19–22 Sept. 2000b.

Hernández-Pajares, M., J. M. Juan, J. Sanz, O. L. Colombo, and H. van der Marel, A new strategy for real-time integrated water vapour determination in WADGPS networks, *Geophys. Res. Lett.*, *28*, 3267–3270, 2001.

Lunt, N., L. Kersley, and G. J. Bailey, The influence of the protonosphere on GPS observations: Model simulations, *Radio Sci.*, *34*, 725–732, 1999.

Mannucci, A. J., B. D. Wilson, D. N. Yuan, C. H. Ho, U. J. Lindqwister, and T. F. Runge, A global mapping technique for GPS-derived ionospheric total electron content measurements, *Radio Sci.*, *33*, 565–582, 1998.

Webb, F. H., and J. F. Zumberge, An introduction to GIPSY/OASIS-II, *Tech. Memo. D-11088*, Jet Propul. Lab., Pasadena, Calif., 1997.

Wessel, P., and W. H. F. Smith, New version of the Generic Mapping Tools released, *Eos Trans. AGU*, *76*, 329, 1995.

Wilson, B. D., A. J. Mannucci, and C. D. Edwards, Subdaily Northern Hemisphere maps using an extensive network of GPS receivers, *Radio Sci.*, *30*, 639–648, 1995.

Zumberge, J. F., D. Dong, M. R. Marcin, and D. A. Stowers, Towards a real-time 1-Hz global GPS network, paper presented at International Symposium on GPS, GPS99, Int. Assoc. of Geod., Tsukuba, Japan, 18–22 Oct. 1999.

M. Hernández-Pajares, J. M. Juan, and J. Sanz, GAGE/UPC, Department of Applied Mathematics IV and Applied Physics, Mod. C-3 Campus Nord UPC, E08034, Barcelona, Spain. (manuel@mat.upc.es)

O. L. Colombo, NASA Goddard SFC, Code 926, MD 20771, USA. (ocolombo@geodesy2.gsfc.nasa.gov)

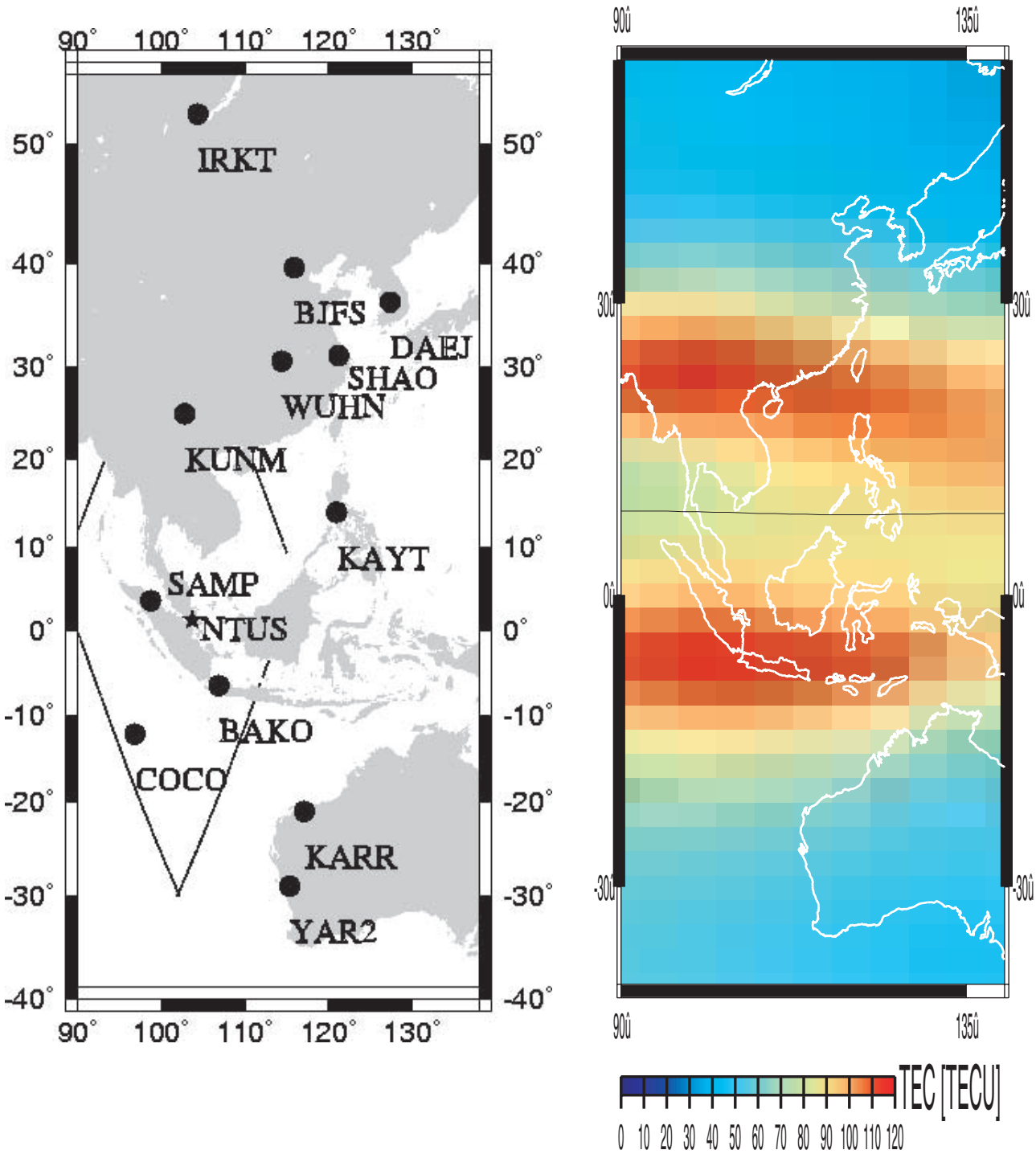


**Figure 3.** Left map: IGS stations used in the study of precise ionospheric determination, during the four consecutive weeks between March and April 2001 (the TOPEX tracks for the day 67 are also plotted). Right map: The TEC during the local afternoon (07UT, day of year [DOY] 67, March 8th, 2001). The geomagnetic equator is also shown. The units are TECU (1 TECU = 10**16 electrons/m**2 ≃16.3 cm in L1). The Appleton north and south tropical anomalies are clearly present, where the TEC reaches values of more than 120 TECU, compared to 90 TECU between them, and 60 TECU or less in the north and south edges of the map (source: UPC's GIM).

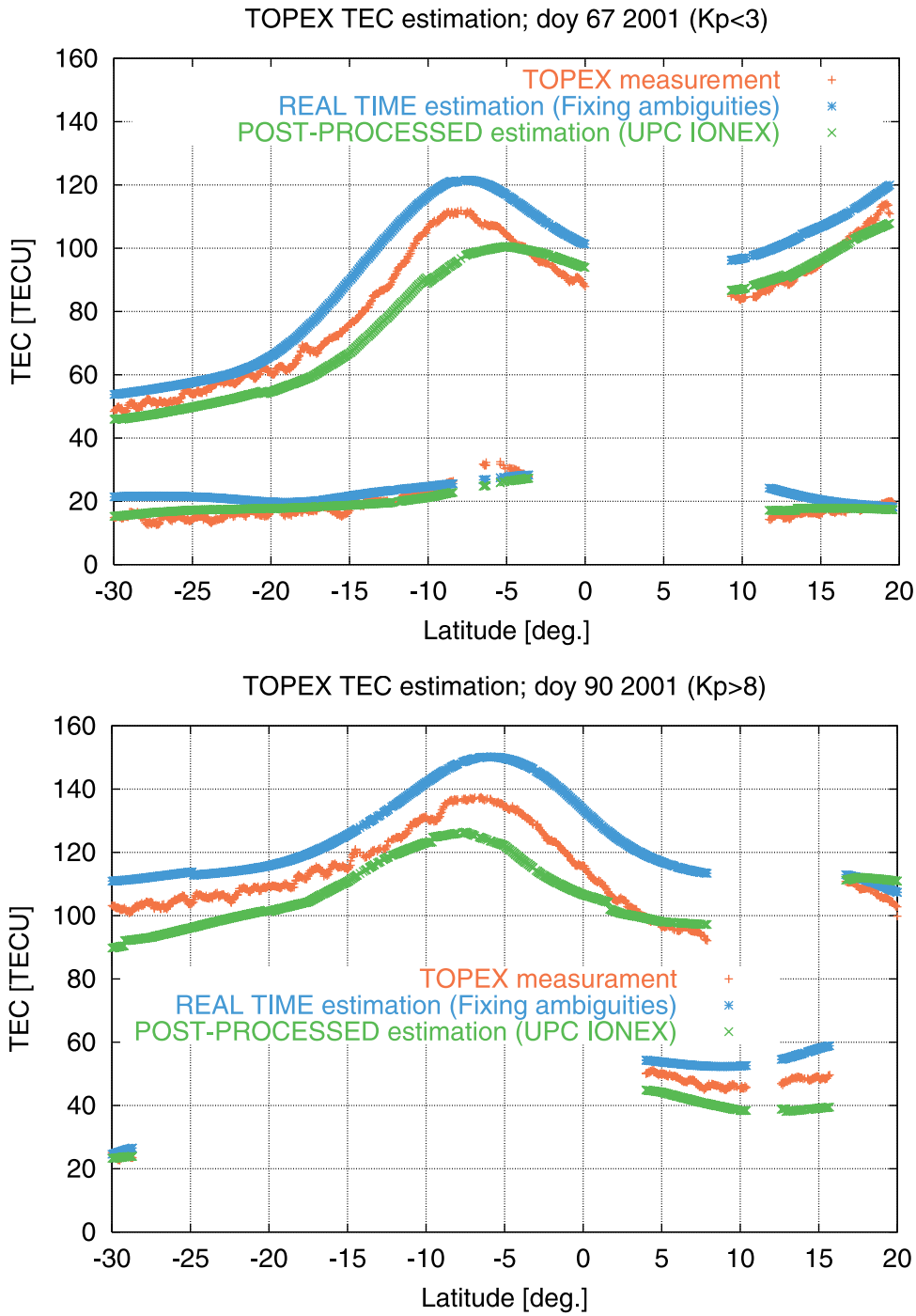


**Figure 5.** Comparison of real-time ionospheric vertical TEC determination, and postprocessed solution, both with GPS data, and TOPEX-derived TEC for four tracks in a geomagnetically quiet day (March 8th, 2001, top plot, see the four TOPEX tracks in Figure 3), and in a day geomagnetically very disturbed, with Kp $\simeq$ 8 (March 31st, 2001, lower plot).